In-phase and anti-phase flagellar synchronization by waveform compliance and basal coupling

To cite this article before publication: Gary S Klindt *et al* 2017 *New J. Phys.* in press https://doi.org/10.1088/1367-2630/aa9031

View the article online for updates and enhancements.

In-phase and anti-phase flagellar synchronization
by waveform compliance and basal coupling

Gary S. Klindt,[1] Christian Ruloff,[2] Christian Wagner,[2,3] and Benjamin M. Friedrich[4, *]

[1]*Max Planck Institute for the Physics of Complex Systems, 01187 Dresden, Germany*

[2]*Experimental Physics, Saarland University, 66041 Saarbrücken, Germany*

[3]*Physics and Materials Science Research Unit,*

University of Luxembourg, 1511 Luxembourg, Luxembourg

[4]*cfaed, TU Dresden, 01062 Dresden, Germany*

(Dated: September 29, 2017)

Abstract

We present a theory of flagellar synchronization in the green alga *Chlamydomonas*, using full treatment of flagellar hydrodynamics and measured beat patterns. We find that two recently proposed synchronization mechanisms, flagellar waveform compliance and basal coupling, stabilize anti-phase synchronization if operative in isolation. Their nonlinear superposition, however, can stabilize in-phase synchronization for suitable parameter choices, matching experimental observations. Our theory is based on a description of the flagellar beat as a limit-cycle oscillator, which was introduced and calibrated by experimental data in a recent letter (Klindt et al., *Phys. Rev. Lett.* 2016). Using a minimal model of basal coupling, we identify regimes of in-phase, anti-phase and even out-of-phase synchronization with spontaneous symmetry-breaking in this system of two identical coupled oscillators as a function of an effective strength of basal coupling. From our theory, we quantitatively predict different synchronization dynamics in fluids of increased viscosity or external flow, suggesting a non-invasive way to control synchronization by hydrodynamic coupling.

*Electronic address: benjamin.m.friedrich@tu-dresden.de

1

I. INTRODUCTION

Pairs of coupled oscillators can synchronize with a fixed phase difference, a phenomenon first observed by Huygens for a pair of pendulum clocks [1]. Since then, synchronization has been described for many physical systems, including beating flagella [2], pairs of heart muscle cells [3], or light-driven microrotors [4].

In each of these different systems, the dynamics towards a synchronized state is well approximated by the classic Adler equation for the phase difference δ between two weakly coupled oscillators [5], which reads (for the simplest case of identical intrinsic frequencies $\omega_0 = 2\pi/T$)

$$\dot{\delta} = -\frac{\lambda}{T}\sin\delta, \quad \delta_{\mathrm{IP}}^* = 0, \quad \delta_{\mathrm{AP}}^* = \pi. \tag{1}$$

The two steady states of Eq. (1), δ_{IP}^* and δ_{AP}^*, characterize in-phase synchronization (IP) and anti-phase synchronization (AP), respectively, see Fig. 1. The sign of the effective synchronization strength λ selects which state is stable. Unless the oscillator coupling possesses special symmetries, λ is generically non-zero [6, 7]. Its sign, however, depends on non-generic features of the system. For example, for a system of two beating metronomes on a moving tray – a modern day analogue of Huygens' pendulum clocks – both IP and AP synchronization were observed, depending on subtle features like friction with the floor [8]. Eq. (1) can be generalized in a straight-forward manner to account for noise [9]. In the presence of noise, the phase difference δ will fluctuate around the stable steady state δ^* of the noise-free equation (with occasional phase-slips). The fluctuation amplitude is set by a competition between the strength of noise and the synchronization strength λ, which is thus the key parameter to be predicted by theory.

At the microscopic scale of biological cells, cilia and flagella represent a prime example of a chemo-mechanical oscillator. Molecular motors inside the flagellum drive regular bending waves of these slender cell appendages [11], rendering the flagellar beat a stable limit-cycle oscillator [12–14]. Single flagella can phase-lock to external oscillatory flows [15]. Pairs of flagella can synchronize their beat, e.g. in the green alga *Chlamydomonas* that swims with $n = 2$ flagella like a breast-stroke swimmer [16–18]. IP synchrony of its two flagella is a prerequisite for swimming straight and fast. The basal bodies of the two flagella are connected by a so-called distal striated fiber [19]. More complex flagellar gaits were observed in species with $n = 2^k$ flagella, with matching patterns of basal coupling [10]. On epithelial

2
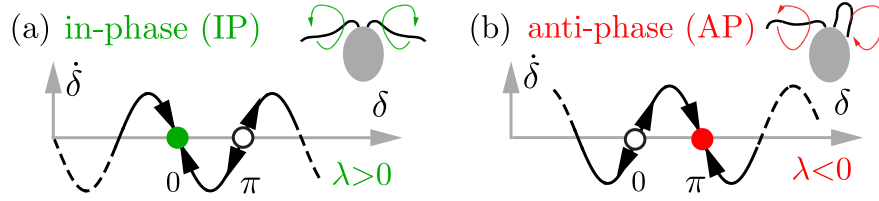
FIG. 1: In-phase and anti-phase synchronization. (a) The generic Adler equation, Eq. (1), predicts stable in-phase synchronization for a pair of coupled oscillators with phase difference $\delta = 0$ for synchronization strength $\lambda > 0$, corresponding to "breast-stroke swimming" *Chlamydomonas*. (b) For $\lambda < 0$, anti-phase synchronization is stable, corresponding to a "free-style gait" [10].

surfaces, $n \gg 10^2$ flagella phase-lock their beat, thus forming metachronal waves [20], which facilitates efficient fluid transport [21–23]. Flagellar synchronization has been studied intensively in the model organism *Chlamydomonas*, reporting both IP and AP beating. While wild-type *Chlamydomonas* cells usually display IP synchrony, stochastic switching between regimes of stable IP and AP beating has been observed in a flagellar mutant (ptx1) [24]. Another mutant (vfl) with impaired basal coupling displayed lack of coordinated flagellar beating altogether [10, 15].

A long-standing hypothesis states that flagellar synchronization arises from a hydrodynamic coupling between flagella [25], as demonstrated for pairs of flagellated cells held at a distance [26]. A popular minimal model of this phenomenon abstracts from the specific shape of flagellar bending waves and represents each flagellum by a sphere moving along a circular orbit [27–34]. The motion of the left and the right sphere with respective phase angles φ_L and φ_R is described by a balance of forces between active driving forces Q_j and hydrodynamic friction forces

$$Q_j = \Gamma_{jL}\dot{\varphi}_L + \Gamma_{jR}\dot{\varphi}_R, \quad j \in \{L, R\}. \tag{2}$$

Specifically, $\Gamma_{LL}\dot{\varphi}_L$ is the hydrodynamic friction force acting on the left sphere due to its own motion, and $\Gamma_{LR}\dot{\varphi}_R$ represents direct hydrodynamic interactions exerted by the right sphere on the left one. This minimal model highlights the role of symmetry-breaking for synchronization [6, 7, 35]. The minimal model possesses parity-time symmetry (PT), characterized by $\Gamma_{LR}(\varphi_L, \varphi_R) = \Gamma_{RL}(-\varphi_R, -\varphi_L)$, i.e. a spatial parity transformation ($\varphi_L \leftrightarrow -\varphi_R$) gives rise to an equivalent dynamics, but with time-arrow reversed [6, 7, 35]. A time-reversal

3

changes the stability of dynamic steady states, while a spatial transformation does not. Thus, there can be neither stable nor unstable synchronized states, unless PT-symmetry is broken.

A number of different PT-symmetry breaking effects have been proposed in the past, including interaction with boundary walls [27], phase-dependent driving forces $Q_j(\varphi)$ [29], and amplitude compliance with a variable radius $A(t)$ of each circular orbit, constrained by an elastic spring [28, 36]. In addition to direct hydrodynamic interactions between the two flagella, synchronization independent of hydrodynamic interactions can occur by a coupling between flagellar beating and the resultant motion of the cell [30]. Importantly, two recent experimental studies suggest that in *Chlamydomonas*, an elastic basal coupling connecting the proximal ends of both flagella could play a key role for flagellar synchronization [10, 15]. While each of these proposed mechanisms could in principle account for synchronization, it is not known, which symmetry breaking mechanism dominates in the real biological system. *A priori*, we do not even know if a specific mechanism will stabilize the IP or AP synchronized state.
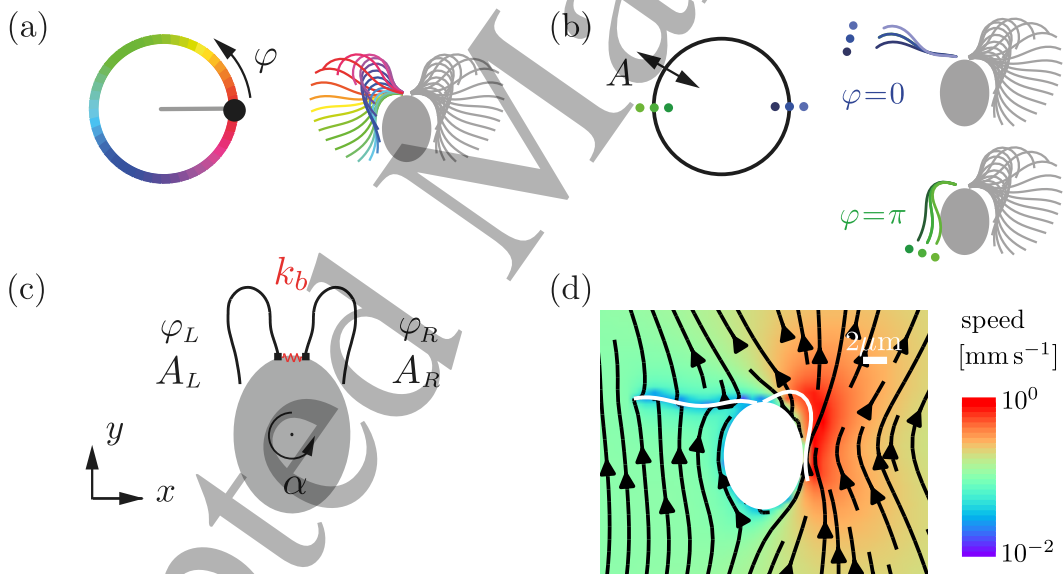
FIG. 2: Theory of flagellar dynamics. (a,b) In our theory, we characterize each flagellum as a limit-cycle oscillator. Each value of oscillator phase φ and amplitude A uniquely determines a flagellar shape [14]. (c) We consider a generic elastic coupling between flagella bases with stiffness k_b, see Eq. (6). (d) Computed hydrodynamic flow field for a change in φ_R ($\dot{\varphi}_R = 2\pi/T$ with $T = 20\,\text{ms}$).

4

Here, we theoretically study flagellar synchronization in the model organism *Chlamy-domonas* to predict conditions for IP and AP synchrony, and present a first experiment to test predictions from our theory. We build on a previously developed description of the beating flagellum as a limit-cycle oscillator, which was calibrated and tested against experimental data [14]. There, we retain the picture of a point moving along a circular orbit. Yet, in our description the point moves in a space of shapes [12, 37]. Each position of the point represents a full shape of the flagellar centerline, see Fig. 2(a,b). Any motion of this point with polar coordinates (φ, A) corresponds to an active shape change of the flagellum, for which we numerically compute hydrodynamic friction forces acting on the cell and its two flagella. All parameters in our theoretical description of flagellar beating are estimated from published experimental data [14]. Additionally, two free parameters are introduced in our generic description of basal coupling. We assume identical parameters of both flagella, aiming at a theory that is both simple and quantitative.

We use this theory to elucidate two PT-symmetry breaking effects: flagellar waveform compliance, and basal coupling between both flagella. We find that both PT-symmetry breaking mechanisms have a strong impact on synchronization, but only their combination yields IP synchrony with a synchronization strength sufficient to overcome noise [12, 17].

To the best of our knowledge, this is the first study that systematically addresses the role of flagellar waveform compliance for flagellar synchronization that uses full hydrodynamics and realistic beat patterns, as opposed to minimal models of orbiting spheres [28], as well as a minimal description of basal coupling.

II. THEORY OF FLAGELLAR SWIMMING AND SYNCHRONIZATION

Recently, we introduced an effective theory of flagellar swimming [14]. This theory was formulated for the case of synchronized beating only, and is now extended to the case of asynchronous beating. For technical details, we refer to [14]. The main idea of the theory is to represent the flagellar beat as a limit-cycle oscillator, see Fig. 2(a). This limit-cycle description is independent of the microscopic details of motor control within the flagellum and only comprises parameters that can be directly inferred from experiments. The limit-cycle oscillator is parametrized by a 2π-periodic phase variable φ and a normalized amplitude A, allowing us to account for waveform compliance with a single degree of freedom. The limit-

5

cycle oscillator description is calibrated by experimental data for an experimental reference condition. Here, the reference condition corresponds to a clamped cell that is immersed in a quiescent fluid of dynamic viscosity $\mu_0 = 1.0\,\mathrm{mPa\,s}$ and exhibits IP-synchronized flagellar beating. Measured beat patterns can be projected on the complex plane using a nonlinear variant of principal component analysis, and parameterized by an instantaneous phase $\varphi(t)$ and amplitude $A(t)$ [14]. This parameterization can always be chosen such that for the reference condition, the phase φ obeys $\dot{\varphi} = \omega_0$, where ω_0 denotes the angular frequency of the flagellar beat, while the amplitude A equals a constant steady-state value A_0, if fluctuations are averaged out. We have thus a unique mapping between flagellar shapes and values (φ, A), see also Fig. 2(b). The theory outlined below allows to predict changes in phase speed $\dot{\varphi}$ and amplitude A for any deviation from the reference condition, e.g. for asynchronous beating, external flow, or altered viscosity of the surrounding fluid.

We use this limit-cycle parametrization of the flagellar beat for both the left and right flagellum of a *Chlamydomonas* cell, and describe the motion of this cell in a plane by a state vector $\mathbf{q}$ with seven degrees of freedom, see Fig. 2(c)

$$\mathbf{q} = (\varphi_L, A_L, \varphi_R, A_R, \alpha, x, y)^T. \tag{3}$$

Here, φ_j, A_j with $j \in \{L, R\}$ denote phase and amplitude of the left and right flagellum, respectively, while α, x, y, denote orientation angle and center position of the cell body.

Each change of a degree of freedom will set the surrounding fluid in motion and induce hydrodynamic dissipation, in addition to friction inside the flagella. The hydrodynamic dissipation rate $\mathcal{R}^{(h)}$ can be computed as the surface integral $\mathcal{R}^{(h)} = \int_S d^2\mathbf{x}\, \mathbf{f} \cdot \mathbf{v}$, where S denotes the surface of the cell including its flagella, $\mathbf{v}(\mathbf{x})$ is the surface velocity corresponding to a change $\dot{\mathbf{q}}$ in the degrees of freedom, and $\mathbf{f}(\mathbf{x})$ the resultant hydrodynamic friction force density acting on the surface S. We can express the hydrodynamic dissipation rate $\mathcal{R}^{(h)}$ in terms of generalized velocities $\dot{q}_j$ and conjugate generalized forces $P_j^{(h)}$

$$\mathcal{R}^{(h)} = P_{\varphi_L}^{(h)} \dot{\varphi}_L + P_{A_L}^{(h)} \dot{A}_L + P_{\varphi_R}^{(h)} \dot{\varphi}_R + P_{A_R}^{(h)} \dot{A}_R + P_{\alpha}^{(h)} \dot{\alpha} + P_x^{(h)} \dot{x} + P_y^{(h)} \dot{y}. \tag{4}$$

The definition of the generalized hydrodynamic friction forces $P_j^{(h)}$ follows the framework of Lagrangian mechanics for dissipative systems, using $\mathcal{R}^{(h)}$ as Rayleigh dissipation function [32, 38]. In the limit of zero Reynolds number, applicable to cellular self-propulsion where inertia is negligible [39], hydrodynamic friction forces are linear in the generalized velocities

6

$\dot{q}_j$, $P_i^{(h)} = \Gamma_{ij}^{(h)}\dot{q}_j$ (Einstein summation convention) due to the linearity of the Stokes equation. Explicitly, we have $\Gamma_{ij}^{(h)} = \int_S d^2\mathbf{x}\, \mathbf{f}^{(i)} \cdot \mathbf{v}^{(j)}$, where $\mathbf{f}^{(i)} = \partial \mathbf{f}/\partial \dot{q}_i$ and $\mathbf{v}^{(j)} = \partial \mathbf{v}/\partial \dot{q}_j$ for any friction force density $\mathbf{f}(\mathbf{x})$. Note that the off-diagonal friction coefficients $\Gamma_{ij}^{(h)}$ for $i \neq j$ are generally non-zero, which implies a coupling between the different degrees of freedom.

In addition to hydrodynamic friction, also intraflagellar friction must be considered. The total friction forces P_j conjugate to a degree of freedom q_j can be written as a sum of hydrodynamic friction forces $P_j^{(h)}$ and intraflagellar friction forces $P_j^{(i)}$ that account for dissipative processes inside the flagellum. The total rate of energy dissipation $\mathcal{R}$ is then expressed in terms of generalized velocities $\dot{q}_j$ and the generalized friction forces $P_j = P_j^{(h)} + P_j^{(i)}$, now using $\mathcal{R}$ as Rayleigh dissipation function. Analogously to Eq. (4), we have $\mathcal{R} = P_{\varphi_L}\dot{\varphi}_L + P_{A_L}\dot{A}_L + P_{\varphi_R}\dot{\varphi}_R + P_{A_R}\dot{A}_R + P_\alpha\dot{\alpha} + P_x\dot{x} + P_y\dot{y}$. Energy balance requires that an internal energy reservoir of the cell is depleted at a rate $-\mathcal{R}$.

We now discuss the intraflagellar friction forces. In a first-order approximation, the intraflagellar friction forces are linear in the generalized velocities, $P_i^{(i)} = \Gamma_{ij}^{(i)}\dot{q}_j$. We expect that the intraflagellar friction forces are of a similar magnitude as the hydrodynamic friction forces. For simplicity, we assume that the intraflagellar friction coefficients are proportional to the respective hydrodynamic friction coefficients, i.e. $\Gamma_{ij}^{(i)} = (1 - \eta)/\eta\, \Gamma_{ij}^{(h)}$ for either $i,j \in \{\varphi_L, A_L\}$ or $i,j \in \{\varphi_R, A_R\}$ and $\Gamma_{ij}^{(i)} = 0$ else. One can show that in this simple, one-parameter approximation, the parameter η is equal to the energy efficiency of the flagellar beat for the reference condition, i.e. equals the ratio between the rate $\mathcal{R}^{(h)}$ of mechanical work exerted on the surrounding fluid, and the total rate of energy dissipation $\mathcal{R}$ required to sustain the flagellar beat [14].

The active motion of each flagellum is generated by the collective dynamics of molecular motors inside the flagellar axoneme. We coarse-grain the activity of the molecular motors by active flagellar driving forces $Q_{\varphi_j}(\varphi_j)$ and amplitude restoring forces $Q_{A_j}(\varphi_j)$, $j \in \{L, R\}$. The active forces Q_j balance the hydrodynamic and intraflagellar friction forces P_j. Thus, we have 7 force balance equations that must hold at each instance in time

$$Q_j = P_j, \quad j \in \{\varphi_L, A_L, \varphi_R, A_R, \alpha, x, y\}. \tag{5}$$

Here, the generalized forces Q_x, Q_y, and Q_α represent constraining forces that ensure constraints of motion imposed on the cell. For a freely-swimming cell, force and torque balance imply $Q_x = Q_y = 0$, $Q_\alpha = 0$. For a fully clamped cell, one would impose $\dot{x} = 0$, $\dot{y} = 0$, $\dot{\alpha} = 0$,

7

and determine the constraining forces Q_x, Q_y, Q_α such that the constraints are satisfied. With this calibration, Eq. (5) fully specify equations of motions of flagellar swimming and synchronization. In section VI, we will also consider the case of a clamped cell exposed to external flow parallel to the long axis of the cell, for which we impose $\dot{x} = 0$, $\dot{y} = u$, $\dot{\alpha} = 0$.

Hydrodynamic computations allow us to determine all hydrodynamic friction coefficients $\Gamma_{ij}^{(h)}$ for a given flagellar beat pattern. Here, we employ a triangulated representation of the cell surface and its flagella and use the fast multipole boundary element method fastBEM [40] to compute hydrodynamic friction forces as described in [41]. We use a flagellar beat pattern recorded for the reference condition of a clamped cell with IP-synchronized beat and dynamic viscosity of $\mu_0 = 1.0\,\mathrm{mPa\,s}$ [14]. There, the efficiency parameter has been estimated as $\eta = 0.21 \pm 0.06$ [14]. Additionally, the flagellar driving forces were uniquely calibrated from the requirement $\dot{\varphi}_L = \dot{\varphi}_R = \omega_0$ and $A_L = A_R = A_0$ for the reference case. The amplitude restoring forces Q_{A_j} determine how fast amplitude perturbations $A - A_0$ decay. Here, we assume exponential relaxation with a single relaxation time-scale τ_A for the reference condition, which uniquely determines Q_{A_j} [14]. For $\omega_0 \tau_A \ll 1$, perturbations cannot change the amplitude, while for $\omega_0 \tau_A \gg 1$ the limit cycle may become unstable. An analysis of amplitude fluctuations of the flagellar beat provided an estimate $\tau_A \approx 6\,\mathrm{ms}$ [12]. We now use this theoretical description to predict dynamics after a perturbation of perfect synchrony for different PT-symmetry breaking scenarios.

III. FLAGELLAR WAVEFORM COMPLIANCE

Elastic degrees of freedom such as a flagellar waveform compliance can break PT symmetry in minimal models of hydrodynamically coupled oscillators, and thus allow for synchronization [28]. We tested this general proposition for the specific case of flagellar synchronization in *Chlamydomonas*, using our theoretical description with amplitude degrees of freedom A_L and A_R. We quantify the stability of the IP-synchronized state in terms of an effective synchronization strength λ, generalizing the parameter λ in Eq. (1), such that $-\lambda/T$ equals the cycle-average Ljapunov exponent for the phase difference $\delta = \varphi_L - \varphi_R$. The sign of λ indicates whether IP synchrony is stable ($\lambda > 0$) or not ($\lambda < 0$).

We computed λ for both the case of free-swimming and of clamped cells, see Fig. 3 for $k_b = 0$ (no basal coupling). Details on the numerical computation of λ can be found in

8

Appendix C. Whether a cell can swim freely, or is restrained from moving, can make a substantial difference for flagellar synchronization [18]. The different synchronization dynamics results from a coupling between flagellar beating and a rotation of the whole cell that is possible only for a free-swimming cell. In the absence of flagellar waveform compliance ($\tau_A = 0$) and basal coupling ($k_b = 0$), we find $\lambda \approx 0.06$ for a free-swimming cell, and $\lambda \approx 0$ for a clamped cell, similar to a previous study [18] [51]. Amplitude compliance ($\tau_A > 0$) changes the synchronization strength, yet, surprisingly, destabilizes IP synchrony for free-swimming cells. Next, we study how an elastic basal coupling affects flagellar synchronization.

IV. BASAL BODY COUPLING

In *Chlamydomonas*, the proximal ends of both flagella are connected by a distal striated fiber, comprising an elastic basal coupling [19], see also inset in Fig. 2(c). Previous experimental studies indicate the importance of this basal link for flagellar synchronization [10, 15]. In the following, we account for a finite elastic stiffness of this basal link, for which we assume a Hookian elastic energy

$$U_b = \frac{k_b}{2b_1^2}[b(\varphi_L, A_L, \varphi_R, A_R) - b_0]^2. \tag{6}$$

Here, b represent the elongation of the basal link, which is a function of the flagellar phases and amplitudes. Tracking the basal link, or even the basal portion of the flagella, which extend into the interior of the cell body, is challenging and has not been achieved in experiments to the best knowledge of the authors. We thus lack detailed information on the elongation of the basal link, except that it must be a periodic function of the flagellar phases. Therefore, we make a generic ansatz that comprises a free parameter, a phase shift φ_0, to test different couplings

$$b(\varphi_L, A_L, \varphi_R, A_R) = b_0 + b_1 A_L \sin(\varphi_L - \varphi_0) + b_1 A_R \sin(\varphi_R - \varphi_0). \tag{7}$$

Fig. 9 in Appendix A compares Eq. (7) for the elongation of the distal striated fiber to a phase-dependent distance between two reference points on tracked flagellar shapes outside the cell body. For these reference points, $b_0 \approx 1\,\mu\mathrm{m}$ and $b_1 \approx 100\,\mathrm{nm}$; values for the distal striated fiber will be smaller.

9
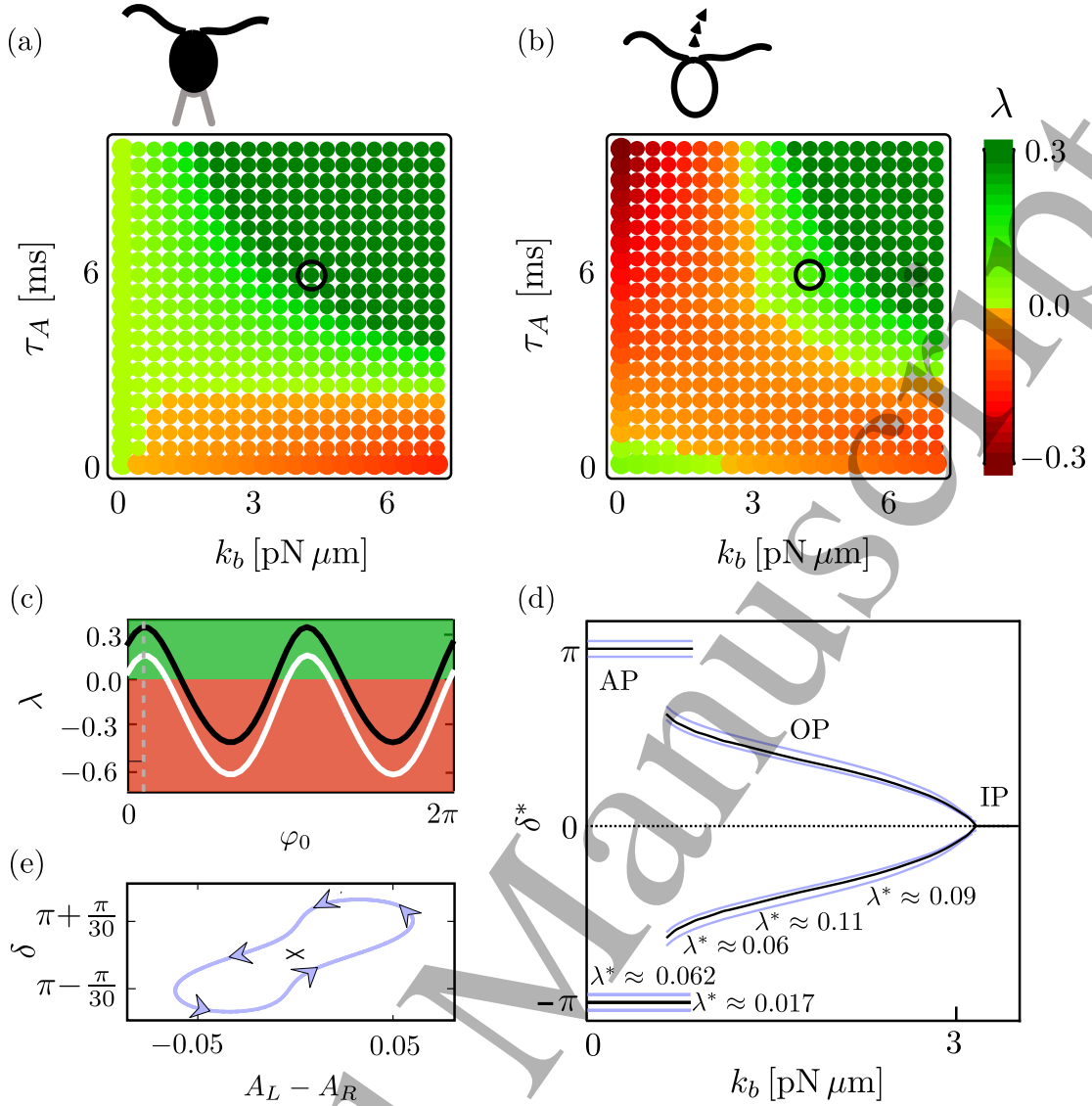
FIG. 3: Waveform compliance and basal coupling jointly determine synchronization dynamics in *Chlamydomonas*. (a) Computed synchronization strength λ (color code) as function of amplitude relaxation time τ_A and basal coupling stiffness k_b for a clamped cell. (b) Same for a free-swimming cell. (c) λ becomes maximal at $\varphi_0 \approx \pi/10$ for both clamped (black) and free-swimming cells (white). (d) Spontaneous symmetry breaking of synchronization: Cycle-averaged phase difference δ^* at steady state as function of basal stiffness k_b computed for a free-swimming cell (black). For selected steady states, we computed synchronization strengths λ^* characterizing Ljapunov exponents $-\lambda^*/T$ of convergence towards δ^*. Blue lines indicate maximum and minimum values of small-amplitude oscillations around δ^* at steady state, see also panel (e), which corresponds to the case $k_b = 0$. Parameters: $T = 20\,\mathrm{ms}$, $\tau_A = 6\,\mathrm{ms}$, $k_b = 4.25\,\mathrm{pN}\,\mu\mathrm{m}$, $\eta = 0.2$, $\mu_0 = 1.0\,\mathrm{mPa\,s}$, $\varphi_0 = \pi/10$, unless stated otherwise.

10

The elastic energy of the basal link results in an additional term in the active flagellar driving force

$$Q_{\varphi_L} \to Q_{\varphi_L} - \frac{\partial U_b}{\partial \varphi_L}_{|\varphi_L, A_L, \varphi_R, A_R} + \frac{\partial U_b}{\partial \varphi_L}_{|\varphi_L, A_L, \varphi_L, A_L}, \tag{8}$$

and similarly for A_L, φ_R, A_R. Here, the last term merely reflects the fact that the elastic basal coupling must be incorporated in the calibration of the flagellar driving forces to yield $\dot{\varphi}_L = \dot{\varphi}_R = \omega_0$ in the reference case of IP-synchronized beating. Note that k_b represents an effective basal coupling strength in Eq. (8). The synchronization dynamics is independent of both b_0 and b_1, yet depends on the unknown phase shift φ_0, see Fig. 3(c).

Fig. 3(a,b) shows numerical results for the synchronization strength λ as a function of basal stiffness k_b for a particular value of φ_0 (such that λ is maximal) for both clamped and free-swimming cells. Remarkably, basal coupling destabilizes IP synchrony in the absence of amplitude compliance, but stabilizes it for realistic values of the amplitude relaxation time τ_A and suitable choice of φ_0. Thus, the combined effect of two PT-symmetry breaking mechanisms is opposite to the sum of their individual effects. A basal stiffness of $k_b = 4.25 \, \mathrm{pN} \, \mu\mathrm{m}$ reproduces a previously measured value of $\lambda \approx 0.3$ for clamped cells [17]. With the length $300 \, \mathrm{nm}$ and cross-sectional area $2 \cdot 10^4 \, \mathrm{nm}^2$ of the distal striated fiber [19], and assuming $b_1 = 50 \, \mathrm{nm}$, our estimate for k_b corresponds to a Young's modulus of approximately $25 \, \mathrm{kPa}$, well in the range of biological materials.

V. OUT-OF-PHASE SYNCHRONIZATION

Flagellar synchronization by basal coupling exhibits dynamics that is more complex then the Adler equation. Fig. 3(d) displays the cycle-averaged phase difference δ^* between both flagella at steady state as a function of basal stiffness k_b. While we find stable AP and IP synchronization for sufficiently weak and strong basal coupling, respectively, consistent with Eq. (1), we find a regime of out-of-phase (OP) synchronization with $0 < \delta^* < \pi$ for intermediate coupling strengths, emerging from the IP-synchronized state by a pitchfork bifurcation. This OP synchronization represents an instance of spontaneous symmetry-breaking with two stable solutions $\pm\delta^*$.

A similar transition from a regime of stable AP synchrony to a regime of stable IP synchrony passing through an intermediate regime of bistable OP synchronization was recently reported in a theoretical study of flagellar synchronization in a pair of short flagella attached

11

to a surface, when their mutual distance was varied [42]. This suggests that bistable synchronization could be a common feature of flagellar synchronization in intermediate regimes between AP and IP synchronization.

VI. SUGGESTIONS FOR EXPERIMENTS

Previous experiments exposed clamped *Chlamydomonas* cells to external flow, reporting a consistent change in phase speed and amplitude of the flagellar beat [14]. This suggests also an altered synchronization dynamics in the presence of external flow. Our theory predicts that for external flow parallel to the long axis of a *Chlamydomonas* cell, the synchronization strength λ is reduced, see Fig. 4(a). This points towards a non-invasive way to control flagellar synchronization.

To probe these predictions, we performed experiments as in [14], exposing *Chlamydomonas* cells held in micropipettes to external flow. Details on experimental methods and data analysis are presented in Appendix A. In short, the Adler equation in the presence of noise, Eq. (A1), predicts a statistical distribution $p(\delta)$ of the phase-difference δ between the two flagella that depends on ratio between the synchronization strength λ and an effective noise strength D. By analyzing the distribution of phase-differences in experiments, we determined the dimensionless ratio $\lambda/(DT)$ as a function of flow rate, see Fig. 4(b). We observe a significant reduction in normalized synchronization strength in 3 out of 6 cells analyzed. Previous independent measurements reported $DT \approx 0.1 - 0.2$ [12, 43], allowing us to compare theoretical predictions and measurements. At the same time, the frequency difference between both flagella stayed approximately constant as a function of flow rate u, see Fig. 4(c). While these experiments are not yet conclusive to prove the role of basal coupling for flagellar synchronization, they provide an intriguing first link between our quantitative theory and experiments.

As a second way to perturb flagellar dynamics, classical experiments demonstrated that an increase in the viscosity of the surrounding fluid slows down the flagellar beat and decreases its amplitude [44]. This suggests also a change of synchronization dynamics. Indeed, our theory predicts a reduction of the synchronization strength upon an increase in fluid viscosity. Fig. 5 shows a computed synchronization strength λ as a function of the dynamic viscosity μ of the surrounding fluid. These theory predictions could be tested in future experiments.

12
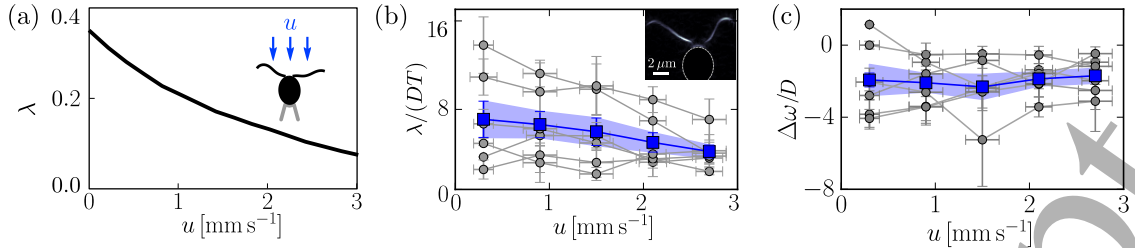
FIG. 4: Control of flagellar synchronization by external flow. (a) Theory: computed synchronization strength λ as function of external fluid flow with velocity u parallel to the long axis of the cell. (b,c) Experiment: measured synchronization strength $\lambda/(DT)$, normalized by effective noise strength D, and normalized difference $\Delta\omega/D$ of intrinsic beat frequencies of both flagella. (blue: mean±s.e.m., $n = 6$ cells; gray: mean±s.e. for individual cells). Parameters for theory, see Fig. 3.

Conceptually, imposing an external flow is equivalent to changing the phase-dependence of the flagellar driving forces. Specifically, an external flow parallel to the long axis of the cell body will accelerate the effective stroke of the beat cycle (when flagella move in the direction of flow), and decelerate the recovery stroke (during which flagella move opposite to the direction of flow). An analogous effect can be achieved by increasing the flagellar driving force Q_φ during the effective stroke and reducing Q_φ during the recovery stroke. Similarly, increasing the viscosity of the surrounding fluid reduces the magnitude of elastic coupling relative to viscous coupling. Thus, increasing the viscosity is formally equivalent to a reduction of the elastic constants.

VII.   MINIMAL MODEL OF SYNCHRONIZATION BY BASAL COUPLING

To gain insight into basic mechanisms of IP and AP synchronization, we revisit a popular minimal model of hydrodynamic synchronization [27–29]. Our aim is to show analytically that the superposition of two synchronization mechanisms that stabilize AP-synchrony if operative in isolation can result in stable IP synchrony as a result of nonlinear effects.

In the minimal model, two spheres of equal radius r move inside a viscous fluid of viscosity μ along circular orbits $\mathbf{r}_j$ of respective radii A_j, with centers separated by a distance d,

$$\mathbf{r}_L = A_L\mathbf{n}_L(\varphi_L) - d\mathbf{e}_x/2, \quad \mathbf{r}_R = A_R\mathbf{n}_R(\varphi_R) + d\mathbf{e}_x/2, \tag{9}$$

13
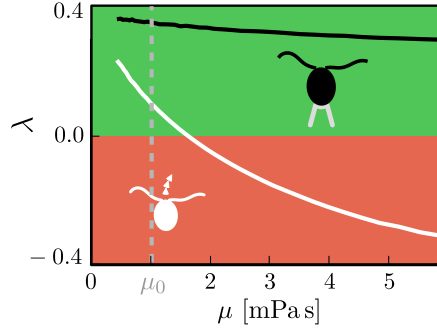
FIG. 5: *Flagellar synchronization in fluids of increased viscosity.* Computed synchronization strength λ as function of the dynamic viscosity μ of the surrounding fluid for clamped (black) and free-swimming cell (white). All parameters except μ as in Fig. 3. The value $\mu_0 = 1.0\,\text{mPa\,s}$ used in Fig. 3 is indicated (dashed line).

see Fig. 6. Here, $\mathbf{n}_j(\varphi_j) = \cos\varphi_j\,\mathbf{e}_x + \sigma_j\sin\varphi_j\,\mathbf{e}_y$ denote radial vectors for $j \in \{L, R\}$ with $\sigma_L = -1$, $\sigma_R = 1$. Each sphere is driven by a constant tangential driving force $Q_j = q_0$ with $q_0 = A_0^2\gamma\omega_0$, friction coefficient $\gamma = 6\pi\mu r$ and reference amplitude A_0. Hydrodynamic interactions couple the motion of both spheres. In the limit $r \ll d$ with A_0/r of order unity, $\Gamma_{LR}\dot\varphi_R = -A_L\gamma^2\,\mathbf{t}_L\cdot\mathcal{G}(\mathbf{r}_L-\mathbf{r}_R)\cdot\dot{\mathbf{r}}_R$, and vice versa. Here, $\mathbf{t}_j = \partial\mathbf{n}_j/\partial\varphi_j$ is the tangent vector and $\mathcal{G}(\mathbf{r}) = (8\pi\mu)^{-1}[|\mathbf{r}|^{-1} + \mathbf{r}\otimes\mathbf{r}/|\mathbf{r}|^3]$ denotes the Oseen tensor. For constant amplitude, $A_i = A_0$, the system possesses PT-symmetry and no net synchronization occurs [6, 7, 27]. Introducing amplitude compliance, $\gamma\dot{A}_L = -k_A(A_L - A_0) - \gamma^2\mathbf{n}_L\cdot\mathcal{G}(\mathbf{r}_R - \mathbf{r}_L)\cdot\dot{\mathbf{r}}_R$ with amplitude stiffness k_A for the left sphere and similarly for the right sphere, breaks PT-symmetry and results in

$$\lambda_a = -3\pi\,\tau_A\omega_0 r/(4d) + \mathcal{O}(r/d)^2, \tag{10}$$

where $\tau_A = \gamma/k_A$ denotes an amplitude relaxation time, see Appendix B for details. Note that we consider counter-rotating spheres, mimicking a clamped *Chlamydomonas* cell [30, 31], while the originally studied case of co-rotating spheres yields $\lambda_a = 9\pi\,\tau_A\omega_0 r/(2d) + \mathcal{O}(r/d)^2$ [28]. Analogous to Eq. (8), we can introduce 'basal coupling' in this two-sphere model as a second PT-symmetry breaking mechanism. Specifically, we assume an elastic energy $U_b = k_b|\mathbf{r}_R - \mathbf{r}_L|^2/(2A_0^2)$. This yields a synchronization strength

$$\lambda_b = -\pi\,k_b/q_0 + \mathcal{O}(r/d) \tag{11}$$

in the absence of amplitude compliance with $\tau_A = 0$. Thus, both mechanism imply $\lambda < 0$

14
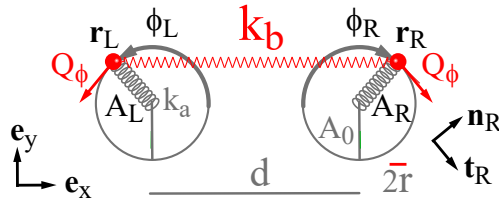
FIG. 6: *Minimal model of hydrodynamic synchronization, accounting for both IP and AP synchrony.* We consider a minimal, analytically tractable model of hydrodynamic synchronization by basal coupling, which abstracts from the detailed model presented in Fig. 2. In the minimal model, two spheres of radius r move along circular orbits of variable radius A inside a viscous fluid of viscosity μ. Each sphere is subject to a tangential driving force Q_φ. An elastic link, mimicking basal coupling, couples the motion of both spheres in addition to hydrodynamic interactions. For the case of counter-rotating spheres, we find that the IP-synchronized state is unstable both in the absence of basal coupling and in the absence of amplitude compliance, but that IP synchrony is stable for the combination of both synchronization mechanisms.

for $r, A_0 \ll d$ if operative in isolation. Their nonlinear superposition, however, results in a positive cross-coupling term

$$\lambda = \lambda_a + \lambda_b + \frac{\pi}{2} \left(k_b/q_0\right)^2 \tau_a \omega_0 + \mathcal{O}(r/d). \tag{12}$$

Thus, $\lambda > 0$ for sufficiently large values of the basal spring stiffness k_b and amplitude relaxation time τ_A. We conclude that the IP-synchronized state is stable in the minimal two-sphere model with counter-rotating spheres for the combination of amplitude compliance and basal coupling, despite the fact that IP synchrony will be unstable for each of these two synchronization mechanisms, if they were operative in isolation. The minimal model thus highlights a key qualitative feature of our detailed theoretical description, and provides analytical insight into the nonlinear superposition of two synchronization mechanisms. Note, however, that the minimal model considers a strongly idealized geometry and is not suitable to make quantitative predictions.

15

VIII.   DISCUSSION

Here, we presented a theory of flagellar swimming and synchronization for the model organism *Chlamydomonas*, to dissect the role of two proposed synchronization mechanisms, flagellar waveform compliance [28] and elastic basal coupling [10, 15]. We find that each mechanism separately stabilized anti-phase synchronization in free-swimming cells, but their combination results in in-phase synchronization, as observed in experiments [16, 17].

Our theory makes specific predictions that can be tested in future experiments. This includes altered synchronization dynamics in the presence of external flow or fluids of increased viscosity. Further, experimental disruption of the distal striated fiber that link the basal bodies of the two flagella, e.g. by laser ablation, could validate the role of basal coupling for synchronization proposed here. While we employed the most simple description of basal coupling, comprising two unknown parameters, future work will have to clarify the elastic properties of the distal striated fiber, and its effect on flagellar synchronization. Intriguingly, previous theories of flagellar beating suggested a crucial role of the boundary conditions at the flagellar base for flagellar dynamics [45, 46].

Our theory is based on a dimensionality-reduced description of the flagellar beat as a limit-cycle oscillator. The parameters of this description were previously estimated from experimental data [14]. This description allows to quantitatively predict responses to external perturbation such as changes in hydrodynamic friction in a generic manner, which is largely independent of modeling assumptions, provided perturbations are sufficiently small. In the future, it will be interesting to incorporate more refined models of flagellar beating, which, however, comprise larger number of parameters and require assumptions regarding the detailed mechanism of motor control [45–49]. Ultimately, we aim to understand conditions for the selection of different synchronized states, such as in flagellar mutants [24, 50].

In conclusion, we have shown that synchronization strengths measured in experiments [17] cannot be explained without basal coupling in the framework of our theory, yet are reproduced for plausible parameter choices assuming such coupling. This suggests an avenue for future experimental and theoretical research.

16

APPENDIX A: EXPERIMENTAL PROTOCOL AND DATA ANALYSIS

We present details for the experiments reported in Fig. 4(b). *Chlamydomonas* cells were held in a micropipette inside a microfluidic device and exposed to controlled microfluidic flow, as described previously [14]. Flow rates were monotonically increased starting from $u = 0 \, \text{mm/s}$. We used only those cells for subsequent analysis, which displayed synchronization in the absence of flow ($u = 0$) and where neither stalling of flagellar oscillations nor a transition to alternate modes of beating occurred for flow speeds up to $u = 3 \, \text{mm/s}$. The proximal segments of both flagella were tracked up to an arc-length position of $2 \, \mu\text{m}$, and automatically corrected for tracking errors. The polar angle of a reference point (located at fixed radial distance from the cell body center) defines a stable sinusoidal signal for each flagellum, see Fig. 7. The Hilbert transform of the mean-corrected sinusoidal signals defines a flagellar phase φ_L and φ_R for the left and right flagellum, respectively. Here, we use the convention that the left flagellum always corresponds to the *cis*-flagellum, as determined from the position of the eye spot of the cell. From the resultant time series, we computed histograms for the distribution of the phase difference $\delta = \varphi_L - \varphi_R$, see Fig. 8(a).

We analyzed this histogram data, using the Adler equation for two weakly coupled oscillators in the presence of both frequency mismatch $\Delta\omega = \omega_L - \omega_R$ between the intrinsic frequencies of the two oscillators and noise, as represented by a noise term $\xi(t)$

$$\dot{\delta} = \Delta\omega - \frac{\lambda}{T} \sin\delta + \xi. \tag{A1}$$

Here, $\xi(t)$ denotes a Gaussian white noise term satisfying $\langle \xi(t)\xi(t') \rangle = 2D\,\delta(t - t')$ with effective noise strength D that sums the noise contribution of both flagella, $D = D_L + D_R$. The steady-state distribution of the phase difference δ according to Eq. (A1) is known as [9]

$$p(\delta) \sim \exp\left(\frac{\lambda}{DT} \cos(\delta) + \frac{\Delta\omega}{D}\delta \right). \tag{A2}$$

We fitted Eq. (A2) to experimental histograms, see Fig. 8(a,b). This provided estimates for the normalized synchronization strength $\lambda/(DT)$ and the normalized frequency mismatch $\Delta\omega/D$, see Fig. 8(c,d).

17
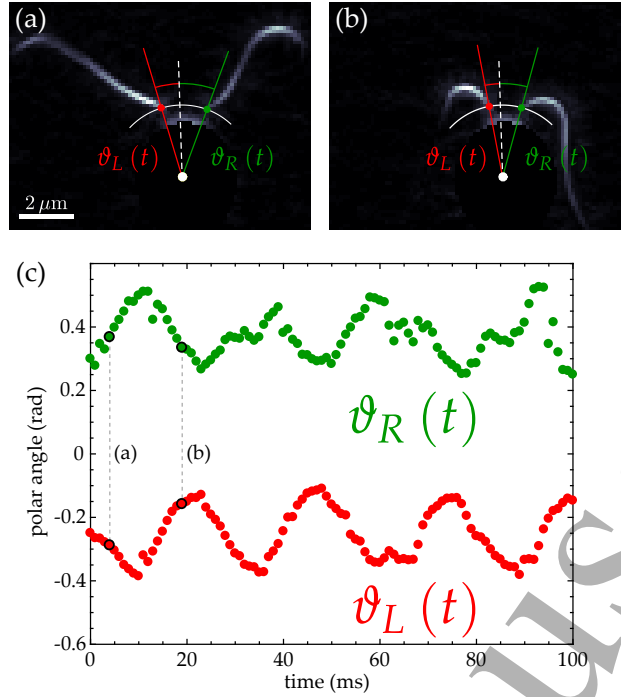
FIG. 7: *Flagellar tracking and determination of flagellar phase* (a,b) For *Chlamydomonas* cells held in a micropipette, reference points were automatically tracked on the proximal segment of both left and right flagellum, and their polar angles $\vartheta_L(t)$ and $\vartheta_R(t)$ with respect to the cell body center at a reference position were computed. Tracking results are shown for effective stroke (a) and recovery stroke (b). (c) The time-dependent polar angles $\vartheta_L(t)$ and $\vartheta_R(t)$ define a stable sinusoidal signal for each flagellum, from which we extracted a flagellar phase for subsequent analysis, see text for details.

APPENDIX B: DERIVATION OF EQUATION (12)

We illustrate the derivation of Eq. (12) for the special case $k_b = 0$ first, which yields λ_a; the general case is treated afterwards.

In the limit of weak coupling between the two spheres, we can separate their dynamics into a fast dynamics of the mean phase $\varphi = (\varphi_L + \varphi_R)/2$ and a slow dynamics of the phase difference $\delta = \varphi_L - \varphi_R$. We further introduce the normalized amplitude difference $a = (A_L - A_R)/A_0$.

We perform a systematic expansion in r/d to derive a coupled system of equations for δ

18
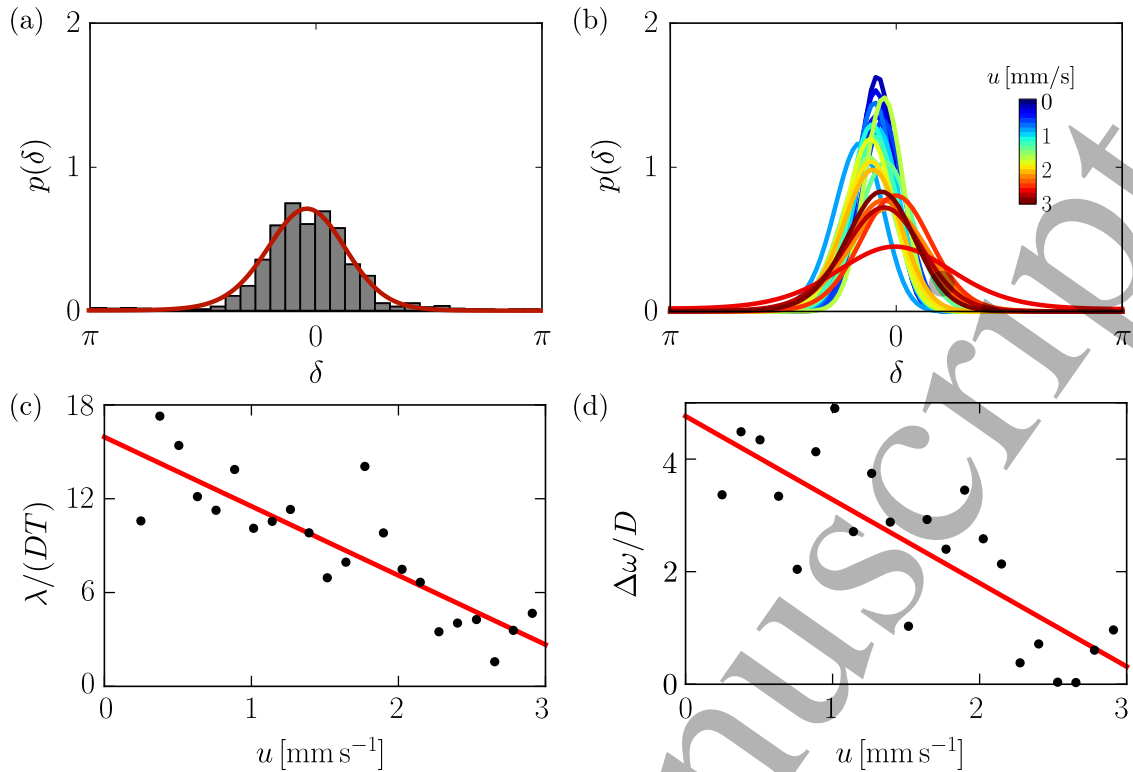
FIG. 8: *Experiments on flagellar synchronization in external flow* (a) Typical histograms of measured phase shifts $\delta = \varphi_L - \varphi_R$ between the left and the right flagellum for *Chlamydomonas* cells exposed to external fluid flow parallel to the long axis of the cell. Fits of the steady-state probability distribution $p(\delta)$ predicted by the Adler equation are shown as solid lines, using Eq. (A2). (b) Shown are resultant fit functions for different flow strengths u (color code) for a single cell. (c) Fits of $p(\delta)$ as shown in (b) provide estimates for $\lambda/(DT)$ and $\Delta\omega/D$, normalized by an effective noise strength D (black). To indicate trends, a linear regression is shown (red).

and a, assuming that δ is small

$$\dot{\delta} = -\omega_0 a + \mathcal{O}\left(\frac{r}{d}a, \frac{r^2}{d^2}\delta\right), \tag{B1}$$

$$\gamma\dot{a} = -k_a a - \frac{3}{8}\frac{r}{d}\gamma\omega_0\,\delta + \mathcal{O}\left(\frac{r}{d}a, \frac{r^2}{d^2}\delta\right). \tag{B2}$$

Eq. (B1) characterizes the non-isochrony of the oscillators, while Eq. (B2) reflects how a non-zero phase shift gives rise to asymmetric amplitude dynamics. Since δ changes slowly with $\dot{\delta} = \mathcal{O}(r/d)$, we obtain from Eq. (B2)

$$a = -\frac{3}{8}\frac{r}{d}\,\tau_A\omega_0\,\delta + \mathcal{O}(r/d)^2, \tag{B3}$$

19
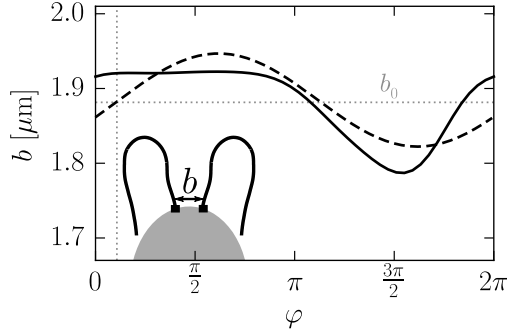
FIG. 9: *Phase-dependent change in basal distance.* From the tracked flagellar beat patterns, we can determine the distance between two reference points on the two flagella at arc-length position $s = 1\,\mu$m close to their fixed basal end point. This phase-dependent distance serves as a proxy for the elongation of the distal striated fiber during in-phase synchronized beating. For comparison, the distance function $b(\varphi, A_L = 1, \varphi, A_R = 1)$ used in our minimal description of basal coupling is shown for comparison (with $\varphi_0 = \pi/10$; b_0 and b_1 do not affect the computation of λ and were obtained by a fit).

where $\tau_A = \gamma/k_a$. The synchronization strength λ can be computed as

$$\lambda = -T \oint \frac{\dot{\delta}}{\delta(0)} d\varphi, \tag{B4}$$

provided $|\delta| \ll 1$. Inserting Eq. (B3) into Eq. (B1) and integrating over one oscillation cycle yields for the case $k_b = 0$

$$\lambda_a = -\frac{3\pi}{4}\, \tau_A \omega_0 \frac{r}{d} + \mathcal{O}(r/d)^2. \tag{B5}$$

We consider a basal coupling with elastic energy

$$U_b = \frac{k_b}{2b_1^2}(b - b_0)^2, \tag{B6}$$

and distance function

$$b = b_0 + b_1 \left[A_L \sin(\varphi_L + \varphi_0) + A_R \sin(\varphi_R + \varphi_0) \right] / A_0, \tag{B7}$$

The choice $\varphi_0 = \pi/2$ corresponds to $U_b = k_b |\mathbf{r}_R - \mathbf{r}_L|^2/(2A_0)^2$ to leading order in r/d. For

20

the case with basal coupling, the dynamic equations for δ and b read

$$\dot{\delta} = -[\omega_0 + \frac{k_b}{2\gamma A_0^2} \sin(2\varphi - 2\varphi_0)]\, a$$

$$+ \frac{k_b}{2\gamma A_0^2}[1 + \cos(2\varphi - 2\varphi_0)]\, \delta + \mathcal{O}(r/d), \tag{B8}$$

$$\gamma \dot{a} = -k_a a + \frac{k_b}{A_0^2} \sin(2\varphi - 2\varphi_0)\, \delta + \mathcal{O}(r/d). \tag{B9}$$

Our assumption of weak coupling between the two spheres corresponds to $k_b \ll A_0^2 \gamma \omega_0$. We obtain from Eq. (B9)

$$a = \text{Im} \frac{1}{1 + 2i\,\tau_A \omega_0}\, \exp(2i\varphi - 2i\varphi_0)\, \frac{k_b}{k_a A_0^2}\, \delta. \tag{B10}$$

For a stiff amplitude spring with $\tau_A \omega_0 \ll 1$, we have $a \approx \sin(2\varphi - 2\varphi_0)\, (k_b/k_a A_0^2)\, \delta$. With Eq. (B4) and Eq. (B8), we conclude

$$\lambda = -\pi \frac{k_b}{q_0} + \frac{\pi}{2} \frac{k_b^2\, \tau_a \omega_0}{q_0^2} + \mathcal{O}(r/d), \tag{B11}$$

where $q_0 = A_0^2 \gamma \omega_0$. Higher-order terms depend on φ_0.

APPENDIX C: COMPUTATION OF SYNCHRONIZATION STRENGTH

We quantify the stability of the IP-synchronized state in terms of a synchronization strength λ

$$\lambda = -\ln \frac{|\delta_{n+1}|}{|\delta_n|}, \tag{C1}$$

where $\delta_n = \delta(t_n)$ denotes the phase difference $\delta = \varphi_L - \varphi_R$ at discrete times t_n for which $\varphi_L = 2\pi n + \varphi$ with initial phase φ. In computations, we use $\delta_0 = 10^{-2}$ and n large enough such that transient dynamics has decayed, while $|\delta| \ll 1$. Computed values for λ occasionally exhibited a weak dependence on φ. Therefore, an average over φ was performed. Applying this definition Eq. (C1) to the Adler equation, Eq. (1), recovers the parameter λ. Generally, the sign of λ indicates whether IP synchrony is stable ($\lambda > 0$) or not ($\lambda < 0$).

For the synchronization strengths λ^* reported in Fig. 2(d), a computed time series $\delta(t)$ was first smoothed using sliding windows of span T and then the function $\delta^* + \Delta \exp(-\lambda^* t/T)$ was fitted (after discarding initial relaxation dynamics), to determine both a cycle-averaged phase difference δ^* and a Ljapunov exponent $-\lambda^*/T$.

21
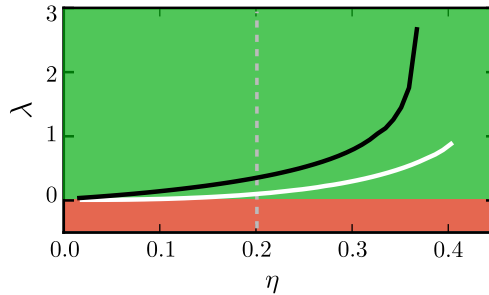
FIG. 10: *Synchronization strength as function of flagellar energy efficiency parameter.* Computed synchronization strength λ increases as function of flagellar energy efficiency parameter η for both clamped (black) and free-swimming cells (white). The value $\eta = 0.2$ used in the main text is highlighted. All other parameters as in Fig. 2 in the main text.

APPENDIX D: DEPENDENCE OF FLAGELLAR SYNCHRONIZATION ON FLAGELLAR ENERGY EFFICIENCY PARAMETER

The synchronization strength λ computed with our theory depends on the flagellar energy efficiency parameter η, see Fig. 10. There, the value $\eta = 0.2$ used in the main text, which was previously determined by a fit of the response of the flagellar beat to uniform external flow [14], is indicated. We find an increase of the synchronization strength λ as a function of η. Similarly, λ converges to zero, as η goes to zero, i.e. if intraflagellar friction becomes much larger than hydrodynamic friction forces. A similar observation was made in a previous study, where phase-locking of the flagellar beat to external oscillatory flows was investigated [14].

[1] A. Pikovsky, M. Rosenblum, and J. Kurths, *Synchronization* (Cambridge UP, 2001).

[2] J. Gray, *Ciliary Movements* (Cambridge Univ. Press, Cambridge, 1928).

[3] I. Nitsan, S. Drori, Y. E. Lewis, S. Cohen, and S. Tzlil, Nat. Phys. (2016).

[4] R. Di Leonardo, A. Búzás, L. Kelemen, G. Vizsnyiczai, L. Oroszi, and P. Ormos, Phys. Rev. Lett. **109**, 034104 (2012).

[5] R. Adler, Proc. IRE **34**, 351 (1946).

[6] G. J. Elfring and E. Lauga, Phys. Rev. Lett. **103**, 088101 (2009).

[7] B. M. Friedrich, Eur. Phys. J. Spec. Top. **225**, 2353 (2016).

[8] J. Pantaleone, Am. J. Phys. **70**, 992 (2002).

[9] R. L. Stratonovich, *Topics in the Theory of Random Noise* (Gordon & Breach, 1963).

[10] K. Y. Wan and R. E. Goldstein, Proc. Natl. Acad. Sci. U.S.A. **113**, E2784 (2016), 1510.03272.

[11] B. Alberts, D. Bray, J. Lewis, M. Raff, K. Roberts, and J. D. Watson, *Molecular Biology of the Cell* (Garland Science, New York, 2002), 4th ed.

[12] R. Ma, G. S. Klindt, I. H. Riedel-Kruse, F. Jülicher, and B. M. Friedrich, Phys. Rev. Lett. **113**, 048101 (2014).

[13] K. Y. Wan and R. E. Goldstein, Phys. Rev. Lett. **113**, 238103 (2014).

[14] G. S. Klindt, C. Ruloff, C. Wagner, and B. M. Friedrich, Phys. Rev. Lett. **117**, 258101 (2016).

[15] G. Quaranta, M. E. Aubin-Tam, and D. Tam, Phys. Rev. Lett. **115**, 238101 (2015).

[16] U. Rüffer and W. Nultsch, Cell Motil. Cytoskel. **41**, 297 (1998).

[17] R. E. Goldstein, M. Polin, and I. Tuval, Phys. Rev. Lett. **103**, 168103 (2009).

[18] V. F. Geyer, F. Jülicher, J. Howard, and B. M. Friedrich, Proc. Natl. Acad. Sci. U. S. A. **110**, 18058 (2013).

[19] D. L. Ringo, Cell **33**, 543 (1967).

[20] M. J. Sanderson and M. A. Sleigh, J. Cell Sci. **47**, 331 (1981).

[21] J. H. E. Cartwright, O. Piro, and I. Tuval, Proc. Natl. Acad. Sci. U.S.A. **101**, 7234 (2004).

[22] N. Osterman and A. Vilfan, Proc. Natl. Acad. Sci. U.S.A. **108**, 15727 (2011).

[23] J. Elgeti and G. Gompper, Proc. Natl. Acad. Sci. U.S.A. **110**, 4470 (2013).

[24] K. C. Leptos, K. Y. Wan, M. Polin, I. Tuval, A. I. Pesci, and R. E. Goldstein, Phys. Rev. Lett. **111**, 158101 (2013).

[25] G. I. Taylor, Proc. Roy. Soc. Lond. A **209**, 447 (1951).

[26] D. R. Brumley, K. Y. Wan, M. Polin, and R. E. Goldstein, eLife **3**, 5030732 (2014).

[27] A. Vilfan and F. Jülicher, Phys. Rev. Lett. **96**, 58102 (2006).

[28] T. Niedermayer, B. Eckhardt, and P. Lenz, Chaos **18**, 037128 (2008).

[29] N. Uchida and R. Golestanian, Phys. Rev. Lett. **106**, 058104 (2011).

[30] B. M. Friedrich and F. Jülicher, Phys. Rev. Lett. **109**, 138102 (2012).

[31] R. R. Bennett and R. Golestanian, Phys. Rev. Lett. **110**, 148102 (2013).

[32] K. Polotzek and B. M. Friedrich, New J. Phys. **15**, 045005 (2013).

[33] M. Theers and R. G. Winkler, Phys. Rev. E **88**, 023012 (2013).

23

[34] Y. Izumida, H. Kori, and U. Seifert, Phys. Rev. E **94**, 052221 (2016), 1602.07116.

[35] J. Elgeti, R. G. Winkler, and G. Gompper, Rep. Prog. Phys. **78**, 056601 (2015).

[36] M. Reichert and H. Stark, Eur. Phys. J. E **17**, 493 (2005).

[37] S. Werner, J. C. Rink, I. H. Riedel-Kruse, and B. M. Friedrich, PLoS One **9**, 1 (2014).

[38] H. Goldstein, C. Poole, and J. Safko, *Classical Mechanics* (Addison-Wesley, Reading, MA, 2002), 3rd ed.

[39] E. Lauga and T. R. Powers, Rep. Prog. Phys. **72**, 096601 (2009).

[40] Y. J. Liu, *Fast Multipole Boundary Element Method: Theory and Applications in Engineering* (Cambridge Univ. Press, Cambridge, 2009).

[41] G. S. Klindt and B. M. Friedrich, Phys. Rev. E **92**, 063019 (2015).

[42] H. Guo, L. Fauci, M. Shelley, and E. Kanso, arXiv:flu-dyn p. arXiv:1708.02181 (2017), arXiv:1708.02181v1.

[43] R. E. Goldstein, M. Polin, and I. Tuval, Phys. Rev. Lett. **107**, 148103 (2011).

[44] C. J. Brokaw, J. exp. Biol. **45**, 113 (1966).

[45] S. Camalet and F. Jülicher, New J. Phys. **2**, 1 (2000), 0003101.

[46] I. H. Riedel-Kruse, A. Hilfinger, J. Howard, and F. Jülicher, HFSP J. **1**, 192 (2007).

[47] C. J. Brokaw, J. exp. Biol. **55**, 289 (1971).

[48] C. B. Lindemann, J. Theor. Biol. **168**, 175 (1994).

[49] P. Sartori, V. F. Geyer, A. Scholich, J. Frank, and J. Howard, eLife **5**, e13258 (2016), arXiv:1511.04270v1.

[50] M. Polin, I. Tuval, K. Drescher, J. P. Gollub, and R. E. Goldstein, Science **325**, 487 (2009).

[51] Reference [18] used $\eta = 1$, implying $\lambda \approx 0.3$, see Fig. 10 in Appendix D.

24